ISSN 0208-7774 TRIBOLOGIA 3/2019 p. 97–106
DOI: 10.5604/01.3001.0013.5440

Katarzyna PIOTROWSKA[*], Monika MADEJ[**], Dariusz OZIMINA[***]

ASSESSMENT OF TRIBOLOGICAL PROPERTIES OF Ti13Nb13Zr TITANIUM ALLOY USED IN MEDICINE

OCENA WŁAŚCIWOŚCI TRIBOLOGICZNYCH STOPU TYTANU Ti13Nb13Zr STOSOWANEGO W MEDYCYNIE

Key words: biomaterials, titanium alloys, surface measurements, surface texture, friction, wear, hip joint.

Abstract

The aim of this study was to evaluate the wear and tear of titanium biomaterials used for hip endoprosthesis. The test materials were samples of titanium and its alloys: Ti grade 4, Ti6Al7Nb and Ti13Nb13Zr. Model tribological tests were carried out in reciprocal motion under conditions of technically dry friction, friction with lubrication provided by an artificial blood solution and Ringer's solution. A 6 mm in diameter Al_2O_3 ball was used as a counter-sample in the friction pairs. After tribological tests, traces of wear were inspected using scanning electron microscopy. A confocal microscope with interferometric mode was used to evaluate the wear of the surface of samples and counter-samples. The lowest friction coefficients among all the material associations were obtained for the Ti13Nb13Zr-Al_2O_3 alloy. SEM analysis has shown that as a result of the wear process, numerous scratches and grooves were generated. They were created as a result of loose products of wear moving around in the friction area. For all tested materials, a pile-up of the wear edges was observed, which indicates an abrasive wear mechanism. During the friction tests of the tested material associations, the titanium disc proved to be the most wearing material. For Ti6Al7Nb and Ti13Nb13Zr alloys, comparable wear was recorded regardless of the test conditions (TDF, AB, RS). The analysis of the obtained tribological results showed that the material association for which the lowest wear of friction pair (sample and counter-sample) recorded was Ti6Al7Nb-Al_2O_3.

Słowa kluczowe: biomateriały, stopy tytanu, pomiary powierzchni, struktura geometryczna powierzchni, tarcie, zużycie, staw biodrowy.

Streszczenie

Celem niniejszej pracy była ocena zużycia biomateriałów tytanowych stosowanych na elementy endoprotezy stawu biodrowego. Materiałem do badań były próbki z tytanu i jego stopów: Ti grade 4, Ti6Al7Nb i Ti13Nb13Zr. Modelowe badania tribologiczne przeprowadzono w ruchu posuwisto-zwrotnym w warunkach tarcia technicznie suchego, tarcia ze smarowaniem roztworem sztucznej krwi oraz roztworem Ringera. Przeciwpróbką w badanych węzłach tarcia była kulka z Al_2O_3 o średnicy 6 mm. Za pomocą elektronowej mikroskopii skaningowej obserwowano ślady wytarcia po testach tribologicznych. Mikroskop konfokalny z trybem interferometrycznym posłużył do oceny zużycia powierzchni próbek i przeciwpróbek. Najmniejsze współczynniki tarcia spośród wszystkich badanych skojarzeń materiałowych uzyskano dla skojarzenia materiałowego–stop Ti13Nb13Zr-Al_2O_3. Analiza SEM wykazała, że w wyniku procesu zużywania generowane były liczne rysy i bruzdy. Powstały one na skutek przemieszczania się luźnych produktów zużycia w obszarze wytarcia. Dla wszystkich badanych materiałów zaobserwowano spiętrzenie obrzeży krawędzi śladów wytarcia świadczące o ściernym mechanizmie zużycia. Podczas testów tarciowych badanych skojarzeń materiałowych najbardziej zużywającym się materiałem była tytanowa tarcza.
W przypadku stopów Ti6Al7Nb oraz Ti13Nb13Zr zarejestrowano porównywalne zużycie bez względu na warunki prowadzenia testów (TDF, AB, RS). Analiza otrzymanych wyników badań tribologicznych wykazała, że skojarzeniem, dla którego zarejestrowano najmniejsze zużycie pary trącej (próbki i przeciwpróbki), było skojarzenie materiałowe Ti6Al7Nb-Al_2O_3.

[*] ORCID: 0000-0001-6366-2755. Kielce University of Technology, Tysiąclecia Państwa Polskiego 7 Avenue, 25-314 Kielce, Poland.
[**] ORCID: 0000-0001-9892-9181. Kielce University of Technology, Tysiąclecia Państwa Polskiego 7 Avenue, 25-314 Kielce, Poland.
[***] ORCID: 0000-0001-5099-6342. Kielce University of Technology, Tysiąclecia Państwa Polskiego 7 Avenue, 25-314 Kielce, Poland.

INTRODUCTION

Modern-age diseases are currently one of the biggest challenges in healthcare. The results of the research presented in the report **[L. 1**] indicate that in the population of people older than 50 years, over 30% of women and 8% of men suffer from motor organ disorders. In the tested group the most frequent were degenerative and discopathic changes in spine and joints,, mainly hip and knee joints. The diseases of the osteoarticular system diagnosed in the research group were causing inflammatory states and pain, and consequently lowered the overall quality of life of patients. According to the report **[L. 2**], degenerative diseases of joints are becoming more common in younger generations. Most often these are caused by straining and degenerative changes in the hip joint resulting from its function, i.e. transferring high static and dynamic loads of the body to the lower limb. For this reason, the hip joint is exposed to deformations and mechanical damage **[L. 3, 4**].

The last few decades have seen significant technological progress in the field of new/modified engineering materials which are considered to be of great importance in the medical field. The leading group of materials used in implantology are metallic materials, with titanium and its alloys being the most commonly used **[L. 5, 6**]. Ti6Al4V and Ti6Al7Nb alloys have been most widely used in orthopaedics. In the research presented by, among others, Qizhi Chen, the harmful effects of aluminium and vanadium on the human body were observed. Vanadium ions caused cytotoxic reactions and neurogenic disorders, while aluminium contributed to softening of bones, as well as brain and blood vessel diseases **[L. 7–9**]. In addition, the mechanical properties of these alloys were questionable, because- they have insufficient resistance to abrasion and corrosion, which leads to loosening of bearing elements of endoprostheses. Therefore, attempts were made to develop new types of titanium alloys, including the Ti13Nb13Zr alloy, in which toxic elements (Al and V) were replaced with biocompatible zirconium and niobium **[L. 10**]. The advantage of the Ti13Nb13Zr alloy lies in its high fatigue strength, a modulus of elasticity similar to that of a human bone, and high resistance to dissolution in tissue and body fluid environments [**L. 11, 12**].

The hip joint is a ball and socket synovial joint with three degrees of freedom of movement, allowing a large range of motion. It consists of the femoral head and the acetabulum. Both surfaces are covered with articular cartilage, which is characterized by high strength, elasticity, and abrasion resistance **[L. 13**]. From the outside, the joint is covered with a thick articular capsule, which is lined with a synovial membrane from the inside. It creates a joint fluid, which moisturizes the articular surface and enables free, smooth movement **[L. 14**]. **Figure 1** shows the elements of the hip joint.

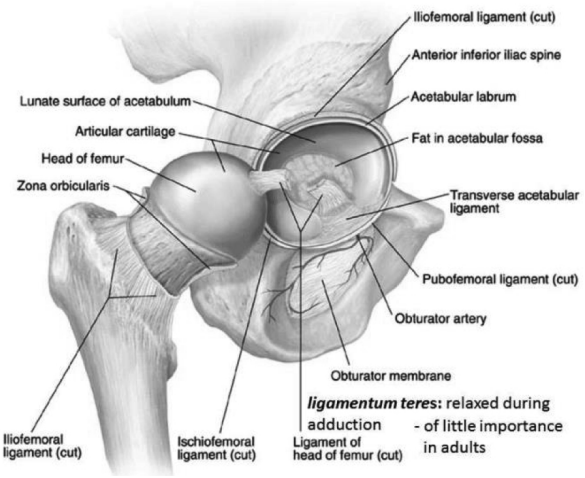

Fig. 1. The elements of the hip joint [L. 15]
Rys. 1. Budowa stawu biodrowego **[L. 15]**

As a result of aging, past diseases and accidents, bone and joint elements deteriorate and the synovial fluid is secreted at a reduced rate. Excessive wear of joints can make active lifestyle impossible. In some cases, the only solution is to perform arthroplasty **[L. 16**]. The aim of the procedure is to substitute the damaged joint elements, along with the products of wear, with an endoprosthesis. Hip joint endoprosthesis consists of a mandrel which replaces part of the femur, head and acetabulum **[L. 17, 18**]. The type of materials used to create the parts of the endoprosthesis affects the wear rate of friction surfaces, as well as the quantity and nature of the generated products of wear. Depending on the frictional associations, the following articulations are distinguished: polyethylene-metal (metal head of the endoprosthesis and polyethylene acetabulum), polyethylene-ceramics (ceramic head and polyethylene acetabulum), metal-metal (metal head and metal acetabulum component), and ceramics-ceramics (ceramic head of the acetabulum and ceramic insert for the acetabulum component) **[L. 16**]. Despite the use of such diverse materials, the wear on the components of endoprostheses is still too heavy. That is why doctors and engineers are constantly working to improve the current hip joint implants, both in terms of the material used and their structure.

The paper presents the results of testing of tribological properties of three titanium materials (Ti, Ti13Nb13Zr, Ti6A17Nb). The tests were carried out under the same conditions and the results were compiled on charts and drawings.

MATERIAL AND METHODS

The materials used in the tests were samples of the following titanium alloys: Ti grade 4, Ti6Al7Nb and Ti13Nb13Zr, the elemental composition of which is listed in **Table 1.**

Table 1. Chemical composition of titanium and its alloy, % wag
Tabela 1. Skład chemiczny tytanu i jego stopów w % wag

Element	C	H	O	N	Fe	Nb	Zr	Al	Ti
Ti	≤ 0.08	≤ 0.015	≤ 0.4	≤ 0.05	≤ 0.5	–	–	–	Based
Ti6Al7Nb	≤ 0.08	≤ 0.015	≤ 0.2	–	–	6.5–7.5	–	5.5–6.5	based
Ti13Nb13Zr	≤ 0.08	≤ 0.015	≤ 0.016	≤ 0.05	≤ 0.25	12.5–14.0	12.5–14.0	–	based

Friction and wear tests were carried out on the TRB³ ball-on-disc tribometer in reciprocal motion. The view of the friction pair is shown on **Fig. 2**. The tribological tests were carried out with the technical and environmental parameters presented in **Table 2**. Balls made of aluminium oxide (III) – Al_2O_3 with a diameter of 6 mm (*Ra* 0.37 μm) were used as the counter-sample material in the friction pairs.

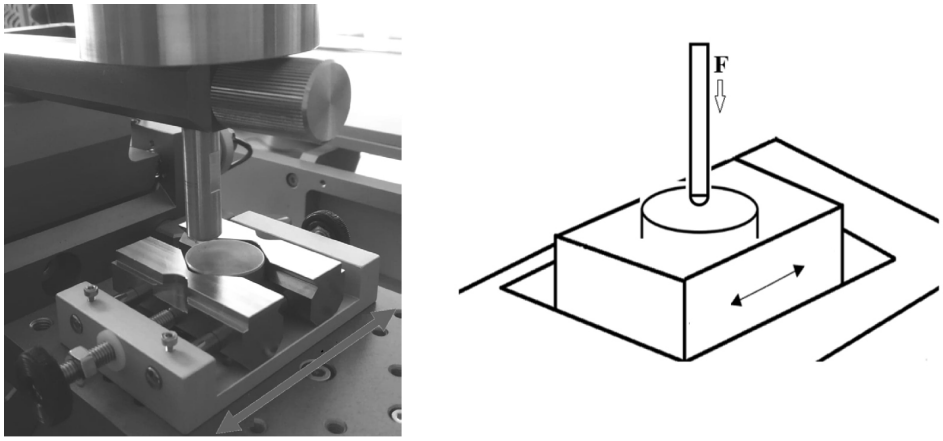

Fig. 2. View of ball-on-disc
Rys. 2. Widok węzła tarcia

Table 2. Technical and environmental parameters of test
Tabela 2. Parametry techniczne i środowiskowe testu

Parameters of test	Unit	Friction pair
		ball Al_2O_3 – disc Ti ball Al_2O_3 – disc Ti6Al7Nb ball Al_2O_3 – disc Ti13Nb13Zr
Load	N	5
Velocity	m/s	0.0159
Cycle	–	10 000
Frequency	Hz	1
Humidity	%	40 ± 5
Temperature	˚C	23±1

Resistance to movement was determined during technically dry friction – TDF and friction using Ringer's solution – RS and blood simulant – AB (**Table 3–4**). The tribological tests were repeated 5 times for each friction pair at the set parameters.

Table 3. Chemical composition of artificial blood (AB)
Tabela 3. Skład chemiczny roztworu sztucznej krwi

Chemical composition [g/ dm^3]								[dm^3]
NaCl	$NaHCO_3$	KCl	K_2HPO_4 *$3H_2O$	$MgCl_2$ *$6H_2O$	$CaCl_2$	Na_2SO_4	$(CH_2OH_3)_3$ CNH_2	1 mol HCl
7,996	0,350	0,224	0,228	0,305	0,278	0,071	6,057	0,04

Table 4. Chemical composition of Ringer solution (RS)
Tabela 4. Skład chemiczny roztworu Ringera

Chemical composition [g/ dm^3]		
NaCl	KCl	$CaCl_2$
8,6	0,3	0,243

After the tribological tests, the surface condition was tested using the following devices:
– Phenom XL scanning electron microscope (SEM) (images of abrasion marks), and
– Leica DCM8 confocal microscope with interferometer mode (geometric surface structure analysis).

RESULTS AND DISCUSSION

The research results are presented in the form of comparative charts and images and are summarized in **Figs. 3–14**. **Figure 3** shows the results of the tribological tests.

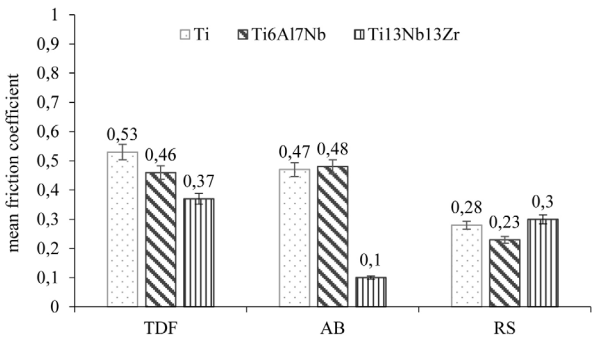

Fig. 3. Mean coefficient of friction during: technical dry friction (TDF), artificial blood (AB) and Ringer solution (RS)
Rys. 3. Średnie współczynniki tarcia podczas: tarcia technicznie suchego (TDF), tarcia ze smarowaniem roztworem sztucznej krwi (AB) oraz roztworem Ringera (RS)

The summary shows that the lowest values of the friction coefficient μ were recorded for tests using Ringer's solution. Their values were comparable for all the materials used. The best tribological characteristics were obtained for the friction association Ti13Nb13Zr--Al_2O_3. In the case of tests carried out under technically dry friction conditions, the obtained μ values were about 20% lower than the values obtained for Ti and Ti6Al7Nb. In turn, in tests with artificial blood solution, they were 80% lower.

After tribological tests, surface morphology observation **(Fig. 4–6**) and analysis of the geometric structure of the surface were conducted **(Fig. 7–9**). The maximum depth and the area of the friction surface determined on the basis of the generated profile of the worn out surface (after tribological tests) were taken as the measure of the sample's wear (**Fig. 10**).

Analysis of the surface of the wear trace (**Figs. 4–6**) indicates that for all alloys tested, the dominant wear mechanism is abrasive wear. This is due to the different properties of the materials from which the friction components/elements have been made. The counter-sample hardness with Al_2O_3 is several times higher than the samples of titanium and its alloys. The scratches and furrows visible in the SEM images were created due to the movement of loose wear products in the friction area. Microcracks were also observed in the signs of wear.

The analysis of the geometric structure of the surface showed that in all the friction pairs there was a uniform surface wear of the top layer. In addition, it was observed that the most wearing material, when paired with an aluminium oxide ball was the titanium disc. For all the materials tested, a pile-up of the wear edges was observed, which indicates an abrasive wear character. In the case of the Ti6Al7Nb and Ti13Nb13Zr alloys, comparable wear was recorded regardless of the conditions of tribological tests (TDF, AB, RS). The wear of Ti13Nb13Zr alloy was about 10% higher in case of technically dry friction and friction with Ringer's solution lubrication and slightly (i.e. 1%) higher in case of friction with artificial blood solution lubrication. Therefore, in biotribological systems, it is possible to replace an alloy containing toxic elements with an alloy with biocompatible elements.

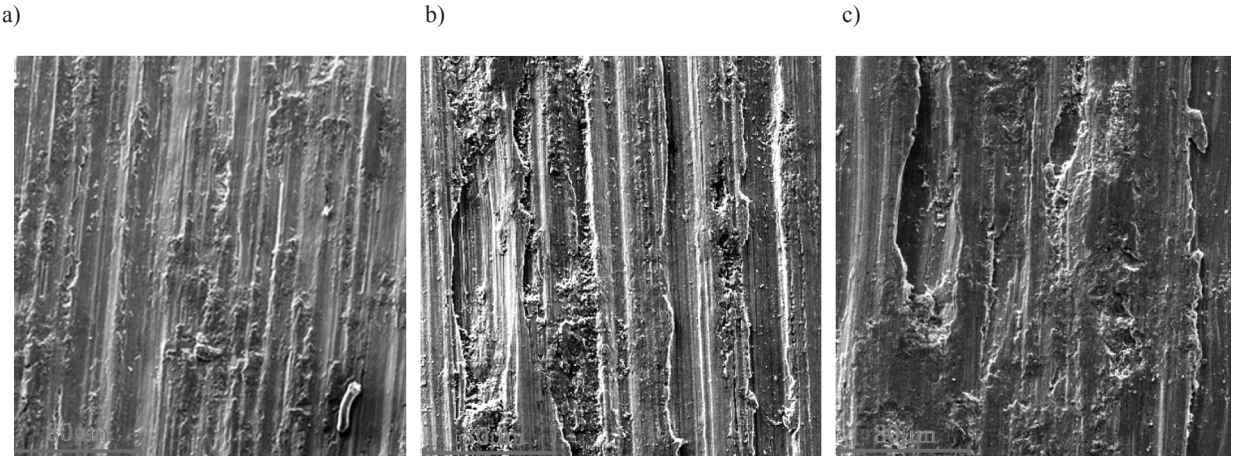

Fig. 4. Surface morphology of the wear traces after TDF: a) Ti, b) Ti6Al7Nb, and c) Ti13Nb13Zr
Rys. 4. Morfologia śladów zużycia po tarciu technicznie suchym a) Ti, b) Ti6Al7Nb, c) Ti13Nb13Zr

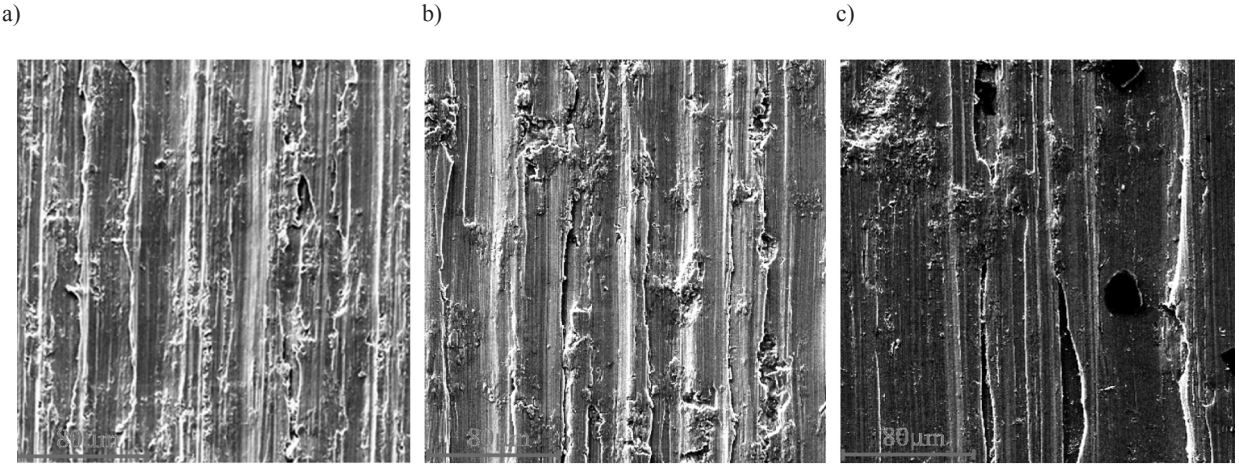

Fig. 5. Surface morphology of the wear traces after friction with AB: a) Ti, b) Ti6Al7Nb, and c) Ti13Nb13Zr
Rys. 5. Morfologia śladów zużycia po tarciu ze smarowaniem roztworem sztucznej krwi a) Ti, b) Ti6Al7Nb, c) Ti13Nb13Zr

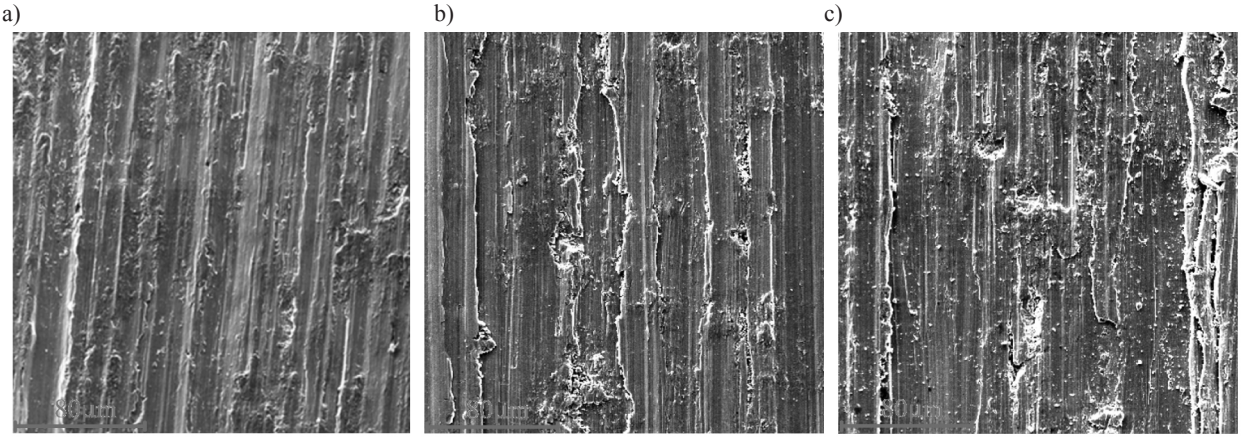

Fig. 6. Surface morphology of the wear traces after friction with RS: a) Ti, b) Ti6Al7Nb, and c) Ti13Nb13Zr
Rys. 6. Morfologia śladów zużycia po tarciu ze smarowaniem roztworem Ringera a) Ti, b) Ti6Al7Nb, c) Ti13Nb13Zr

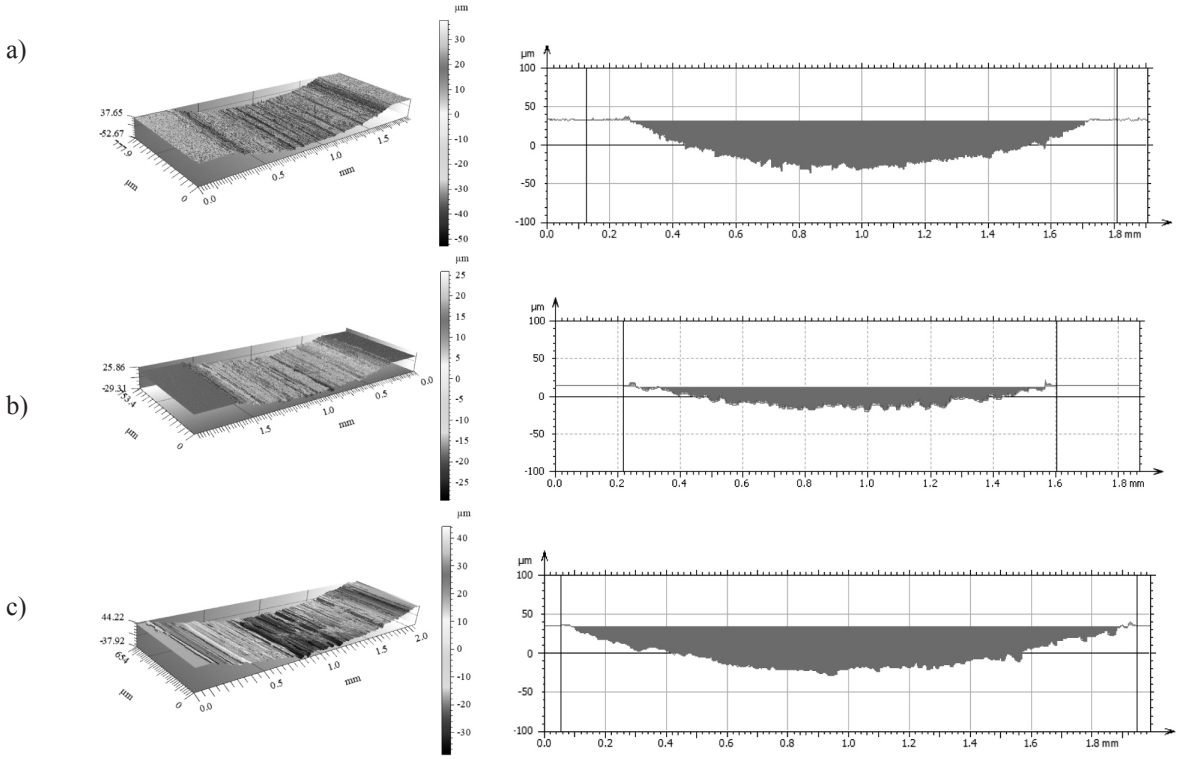

Fig. 7. The isometric images of the wear traces and the wear profile in a cross-section for technically dry friction: a) Ti, b) Ti6Al7Nb, and c) Ti13Nb13Zr

Rys. 7. Obrazy izometryczne śladów wytarcia i profile wytarcia na przekroju poprzecznym podczas tarcia technicznie suchego a) Ti, b) Ti6Al7Nb, c) Ti13Nb13Zr

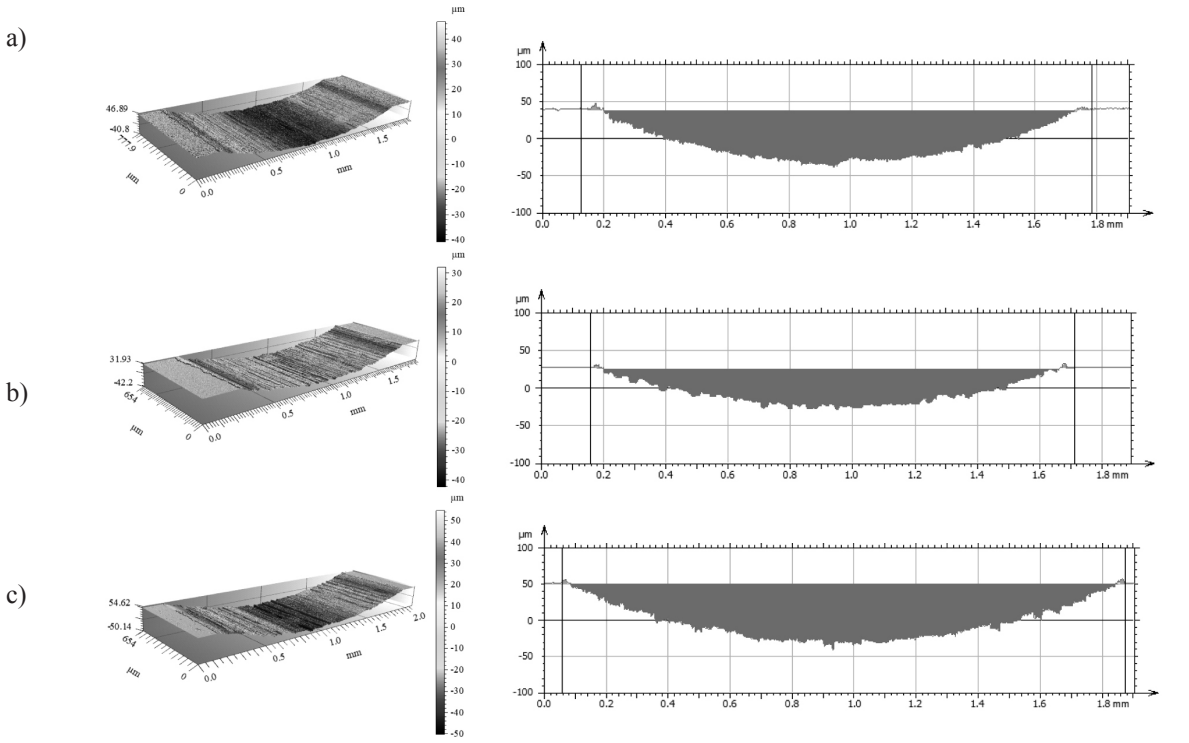

Fig. 8. The isometric images of the wear traces and the wear profile in a cross-section in the conditions lubrication the artificial blood: a) Ti, b) Ti6Al7Nb, and c) Ti13Nb13Zr

Rys. 8. Obrazy izometryczne śladów wytarcia i profile wytarcia na przekroju poprzecznym podczas tarcia ze smarowaniem roztworem sztucznej krwi a) Ti, b) Ti6Al7Nb, c) Ti13Nb13Zr

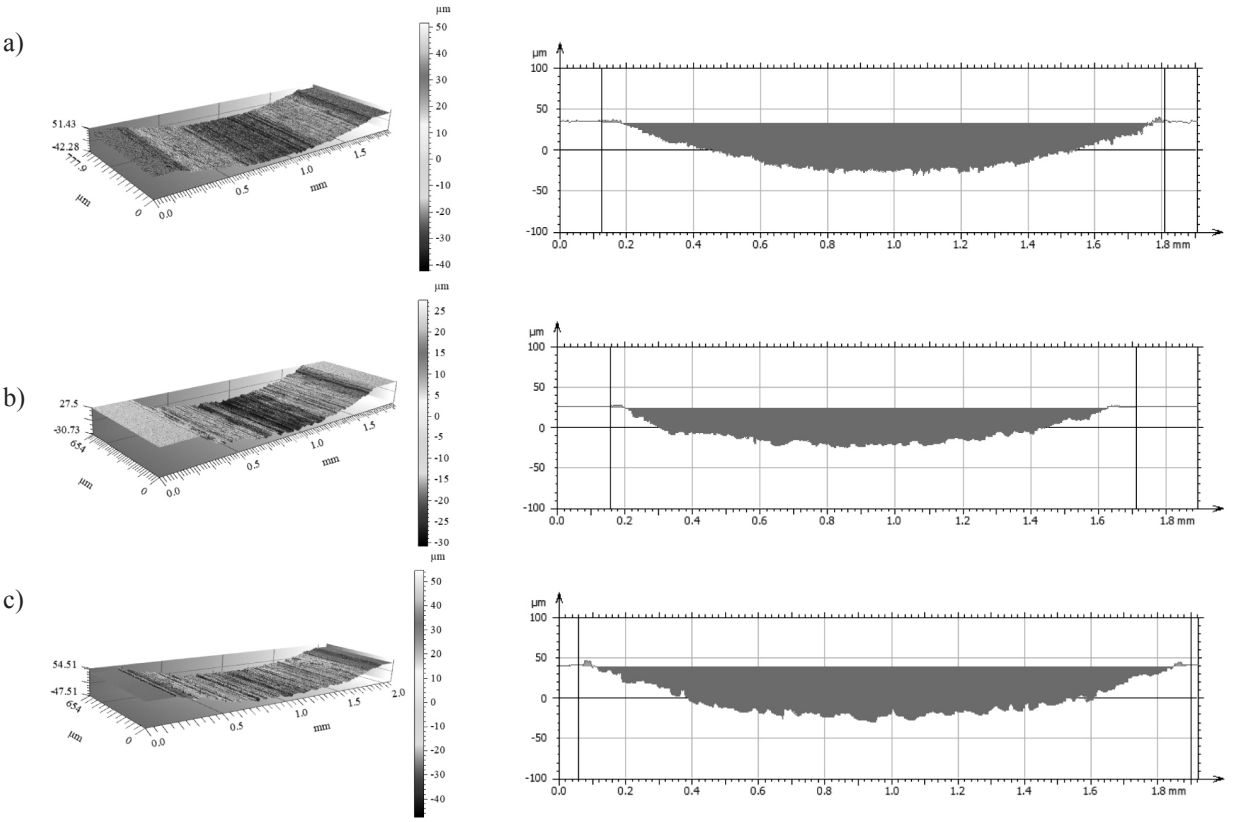

Fig. 9. The isometric images of the wear traces and the wear profile in a cross-section in the conditions lubrication the Ringer's solution: a) Ti, b) Ti6Al7Nb, and c) Ti13Nb13Zr

Rys. 9. Obrazy izometryczne śladów wytarcia i profile wytarcia na przekroju poprzecznym podczas tarcia ze smarowaniem roztworem Ringera a) Ti, b) Ti6Al7Nb, c) Ti13Nb13Zr

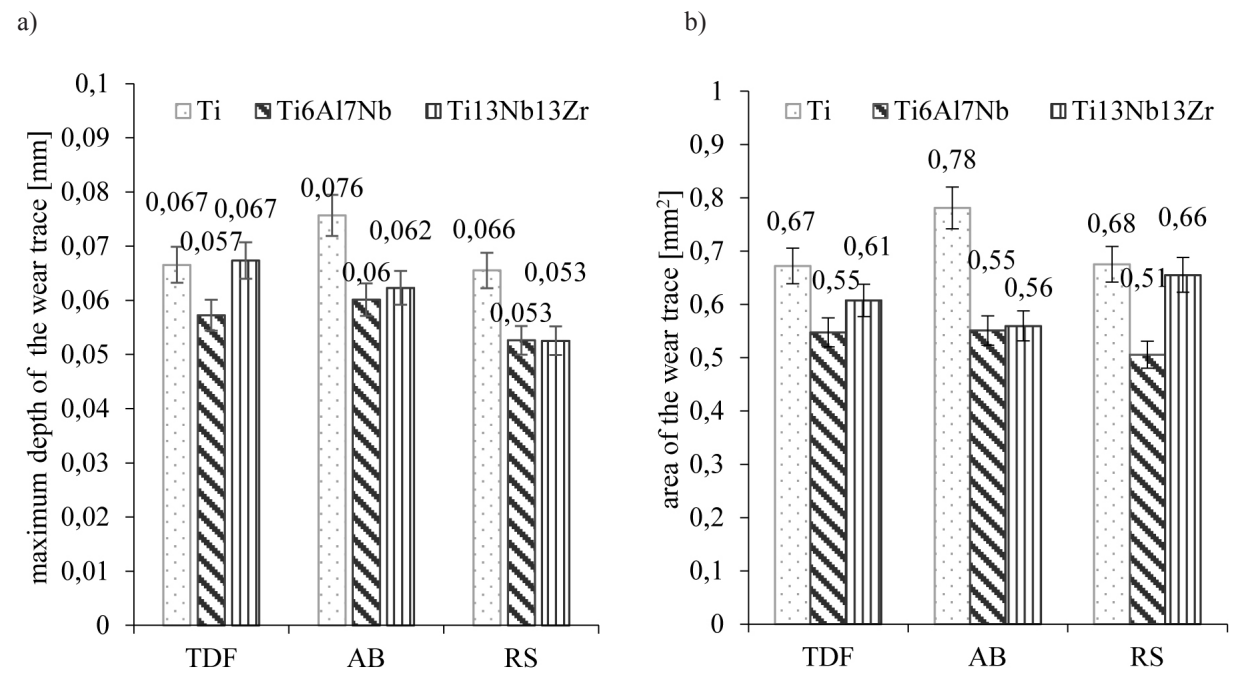

Fig. 10. Maximum depth of the wear (a) and area of wear (b) in a cross-section

Rys. 10. Maksymalna głębokość wytarcia (a) i pole wytarcia (b) na przekroju poprzecznym

Figures 11–13 shows friction marks of counter-samples – Al_2O_3 balls, and **Fig. 14** shows comparative graphs of wear values.

The analysis of the obtained tribological results showed that the material association for which the lowest wear of friction pair (sample and counter-sample)

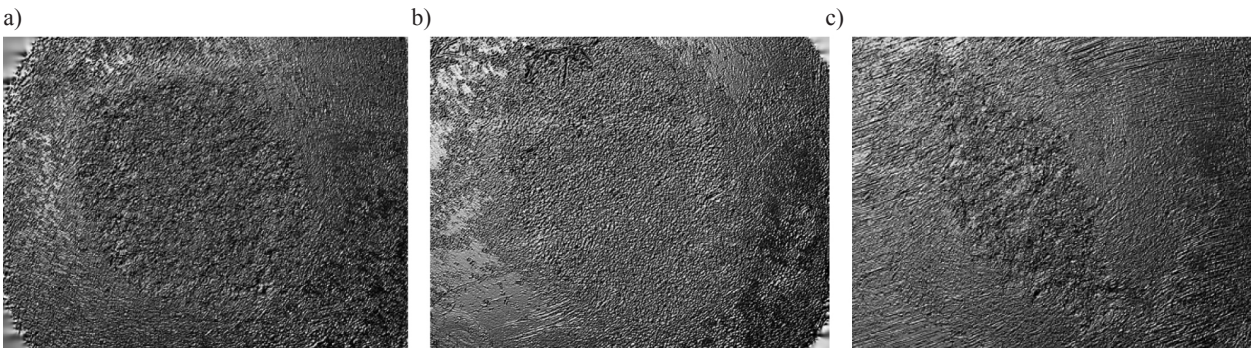

Fig. 11. Images of the wear traces on the Al_2O_3 ball for TDF: a) Ti, b) Ti6Al7Nb, and c) Ti13Nb13Zr
Rys. 11. Obrazy śladów wytarcia kulki Al_2O_3 podczas tarcia technicznie suchego w parze trącej z: a) Ti, b) Ti6Al7Nb, c) Ti13Nb13Zr

Fig. 12. Images of the wear traces on the Al_2O_3 ball in the conditions lubrication the AB: a) Ti, b) Ti6Al7Nb, and c) Ti13Nb13Zr
Rys. 12. Obrazy śladów wytarcia kulki Al_2O_3 podczas tarcia ze smarowaniem roztworem sztucznej krwi, a) Ti, b) Ti6Al7Nb, c) Ti13Nb13Zr

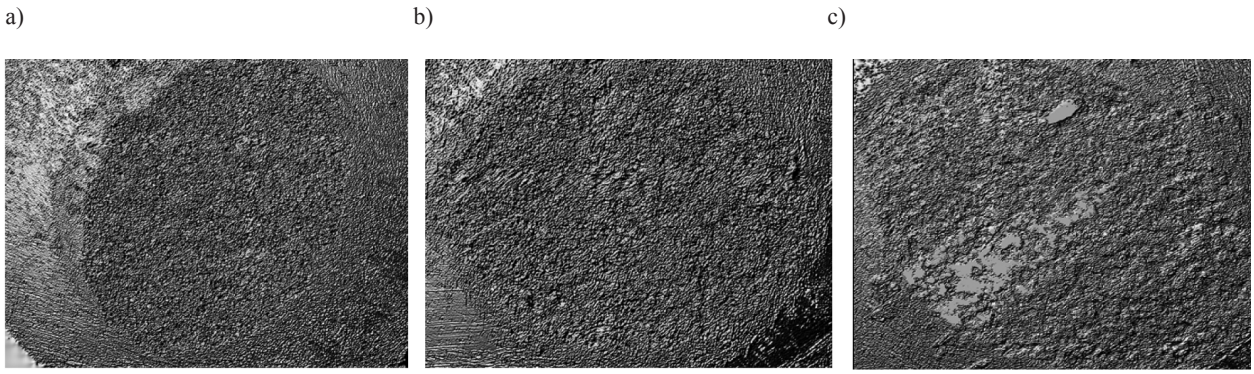

Fig. 13. Images of the wear traces on the Al_2O_3 ball in the conditions lubrication the RS: a) Ti, b) Ti6Al7Nb, and c) Ti13Nb13Zr
Rys. 13. Obrazy śladów wytarcia kulki Al_2O_3 podczas tarcia ze smarowaniem RR, a) Ti, b) Ti6Al7Nb, c) Ti13Nb13Zr

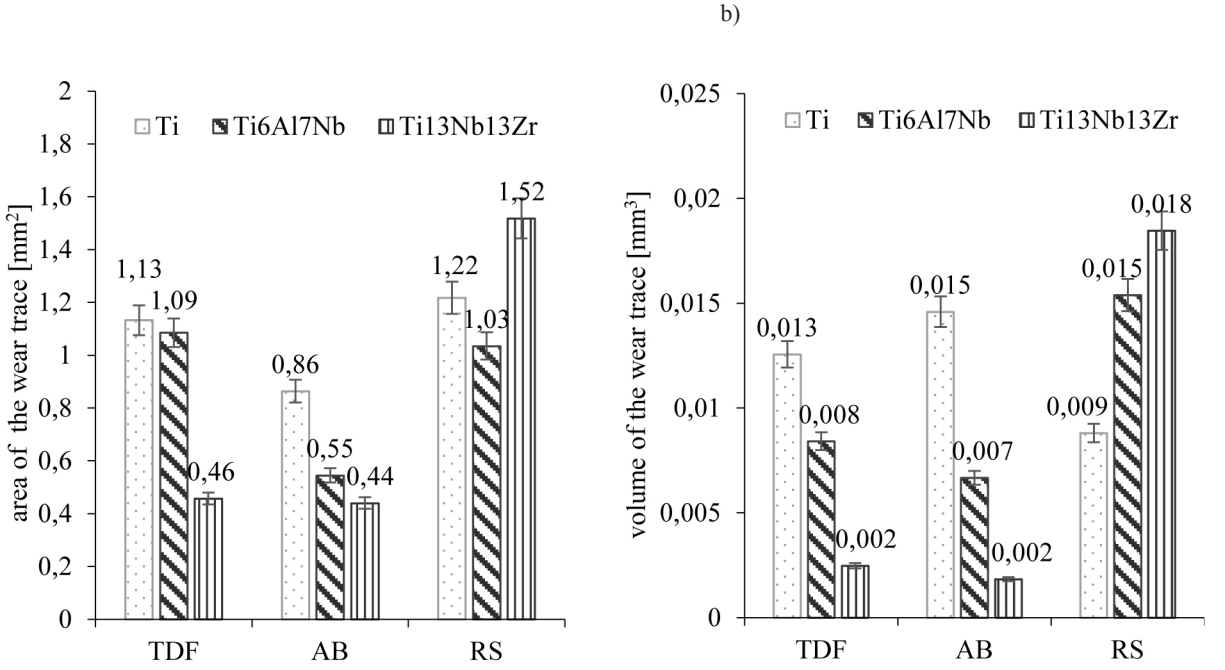

Fig. 14. Area (a) and volume (b) of the wear trace on the Al_2O_3 ball
Rys. 14. Pole (a) i objętość (b) wytarcia przeciwpróbki

was recorded was Ti6Al7Nb-Al_2O_3. For the Ti13Nb13Zr alloy the best tribological characteristics were obtained when lubricated with Ringer's solution. The recorded wear of both the sample and the counter-sample was the lowest of all the friction pairs tested.

CONCLUSIONS

The results of tribological tests showed that the lowest friction coefficients among all the tested friction pair were obtained for the material Ti13Nb13Zr-Al_2O_3. In the case of tests carried out under technically dry friction conditions, the obtained μ – values were about 20% lower than the values obtained for Ti and Ti6Al7Nb. In turn, in tests with artificial blood solution, they were 80% lower. The analysis of the surface of abrasion marks revealed that the wear mechanism of all the tested samples indicates a typically abrasive nature of the wear. SEM images showed scratches and grooves caused by the movement of loose wear elements in the friction zone. Micro-cracks were also observed in wear marks. The analysis of the geometric structure of the surface showed that, in all the friction pairs, there was a uniform surface wear of the top layer of the cooperating elements. For all the materials tested, a pile-up of the wear edges was observed, which indicates an abrasive wear character. The analysis of the obtained tribological results showed that the material association for which the lowest wear of friction pair (sample and counter-sample) was recorded was Ti6Al7Nb-Al_2O_3. The wear of- the Ti13Nb13Zr-Al_2O_3 was comparable to that of Ti6Al7Nb. In summary, the results of abrasive wear resistance studies of selected materials allow considering the replacement of the alloys containing toxic elements with biocompatible Ti13Nb13Zr alloy in orthopaedic applications.

REFERENCES

1. Gajewski T., Woźnica I., Młynarska M., Ćwikła S., Strzemecka J., Bojar I.: Wybrane aspekty jakości życia osób ze zmianami zwyrodnieniowymi kręgosłupa i stawów, Medycyna Ogólna i Nauki o Zdrowiu, 19, 3, 2013, pp. 362–369.
2. Raport: Starzejące się społeczeństwo jako wyzwanie ekonomiczne dla europejskich gospodarek. Internet: http://amcham.pl/file/pdf/raport_starzejace_sie_spoleczenstwo_jako_wyzwanie_ekonomiczne_dla_europejskich_gospodarek.pdf?PHPSESSID=fa061811dd1fda 75f0e9d2867232185f (dostęp: 2019.07.24).
3. Marciniak J.: Biomateriały. Wyd. Pol. Śląskiej, Gliwice, 2002.

4. Niemczewska-Wójcik M., Piekoszewski W.: The analysis of the tribological processes occurring in the socket-and-ball friction pair of a hip joint endoprosthesis, Tribology, 6, 2015, pp. 81–92.
5. Trevisan F., Calignano F., Aversa A., Marchese G., Lombardi M., Biamino S, Ugues D., Manfredi D.: Additive manufacturing of titanium alloys in the biomedical field: processes, properties and applications, Journal of Applied Biomaterials & Functional Materials, 16 (2), 2018, pp. 57–67.
6. Gałuszka G., Madej M., Ozimina D., Kasińska J., Gałuszka R.: The characterisation of pure titanium for biomedical applications, Metalurgija, 56, 1, 2017, pp. 191–194.
7. Rhoads L.S., Silkworth W.T., Roppolo M.L., Whittingham M.S.: Cytotoxicity of nanostructured vanadium oxide on human cells in vitro, Toxicol In Vitro, 2010.
8. Exley C.: The toxicity of aluminium in humans, Morphologie, 2016, pp. 51–55.
9. Chen Q., Thouas G.A.: Metallic implant biomaterials, Materials Science and Engineering: R: Reports, 87, 2015, pp. 1–57.
10. Dąbrowski R.: The microstructure and properties of Ti13Nb13Zr alloy for biomedical applications, Mechanika w medycynie, Rzeszów, 2014, pp. 53–62.
11. Niinomi M.: Materials for biomedical devices, Wood Head Publishing Limited, 2010.
12. Kiryczuk K., Penkała P.: Analiza biomechaniczna stawu biodrowego, Monografia, Maszyny i procesy produkcyjne, Politechnika Lubelska, Lublin, 2015.
13. Gierzyńska-Dolna M., Wiśniewska-Weinert H., Adamus J.: Tribological and material conditionings of the hip endoprostheses application. Tribologia: Tarcie, Zużycie, Smarowanie, 2009, pp. 47–62.
14. https://www.orthobullets.com/recon/12769/hip-anatomy, (dostęp: 2019.07.24).
15. Wendland J., Gierzyńska-Dolna M., Rybak T., Wiśniewski T., Rajchel B.: Investigation for w new biomedical for the hip endoprostheses elements, Obróbka plastyczna metali, XX, 2, 2009.
16. Podwysocka A.: Staw biodrowy: budowy i choroby, Poradnik zdrowie, dostęp: 13.11.2018r, link: https://www.poradnikzdrowie.pl/zdrowie/kregoslup-kosci-stawy/staw-biodrowy-budowa-i-choroby-aa-XLPG-9cGT-Lzbw.html#staw-biodrowy-budowa.
17. Gałuszka R., Madej M., Ozimina D., Krzyszkowski A., Gałuszka G.: The characterisation of the microstructure and mechanical properties of diamond - like carbon (DLC) for endoprosthesis, Metalurgija, 56, 1–2, 2017, pp. 195–198.